Analysis and Modeling of Super-Regenerative Oscillators with FMCW Signals

Sergio Sancho, Mabel Ponton, Almudena Suarez
Universidad de Cantabria, Spain
{sanchosm, mabel.ponton, suareza}@unican.es

***Abstract*—Active transponders based on super-regenerative oscillators (SRO) have the advantages of high gain, low power consumption, and a compact implementation. They are based on a switched oscillator excited by a low amplitude FMCW signal, which provides an approximately phase-coherent response. Due to the system complexity, involving the start-up transient and a time varying phase shift, any realistic modeling is demanding. Here an accurate formulation is presented, which makes use of an instantaneous phase function, extracted through a circuit-level envelope-transient simulation of the standalone SRO in a single quench period. The formulation based on this phase function avoids all the simplifications considered in previous works. It provides the relationship between the baseband frequency and the distance to the target with no need for long time simulations of the transponder system. For illustration, the method will be applied to an SRO at 2.7 GHz, which has been manufactured and measured.**

***Keywords*—envelope transient, super-regenerative oscillator, active transponder.**

I. INTRODUCTION

The work [1] presented a novel type of secondary radar system based on a super-regenerative oscillator (SRO), with ranging and communications capabilities and no need for synchronization with the reader system. The SRO, switched on and off by a quench signal, responds to the interrogation with an approximately phase coherent signal [1], [2] and has the advantages of a low consumption and high gain, mainly due to the oscillator exponential start-up transient [3], [4]. Following [1], [2], other concepts and applications have been proposed [5], [6], [7], [8], [9], including positioning based on multiple backscatter transponders [6] or novel implementations with downmixing capabilities to bust the reception frequency [5]. The operation principles have been demonstrated with theoretical derivations and the benefits have been experimentally confirmed. However, the demonstrations are based on overly idealized models of the switched oscillator, represented as a carrier with a rectangular modulation amplitude. Instead, the envelope of the switched oscillation will depend on the dynamics of the particular circuit. In previous models, the phase difference with respect to the input signal is assumed to be a linear function of time, whereas the oscillator frequency undergoes instantaneous variations during the transient to the steady state. Though the simplified analyses provide an insightful description of the transponder operation, they will be insufficient for the realistic prediction of the SRO behavior.

In this work we present a realistic formulation of an SRO transponder with ranging capability. It relies on a nonlinear phase function $\gamma(t,\omega)$, depending on time and the excitation frequency ω, which can be extracted through a simple circuit-level envelope-transient simulation of the standalone SRO in a single quench period. This function is used to predict the SRO response to a FMCW interrogation signal, as well as the reader baseband output, which provides the distance to the target. The new formulation avoids all the previous simplifications and enables an efficient computation of the baseband output. As will be shown, the results are in excellent agreement with costly circuit-level envelope-transient simulations, carried out during the long-time intervals required for the range calculation. For illustration, the method will be applied to an SRO at 2.7 GHz, which has been manufactured and measured.

II. NONLINEAR PHASE FORMULATION

The schematic of the SRO transponder system is shown in Fig. 1. The base station transmits a linear stepped-frequency modulated signal:

$$v_{RF}(t) = V_{RF}\cos\phi_{RF}(t), \tag{1}$$

where V_{RF} is a constant amplitude and the instantaneous frequency $\dot{\phi}_{RF}(t)$ grows in steps $\Delta\omega = \mu\Delta T$ of time-length ΔT. In an interrogation cycle, it can be expressed as $\dot{\phi}_{RF}(t) = \omega_{RF,k} = \omega_o + \mu(k-N)\Delta T$ for $t \in [k\Delta T, (k+1)\Delta T)$, where ω_o is the free-running frequency of the transponder oscillator, and $k = 0, \ldots, 2N$ (Fig. 1). As explained in [1], the overall modulation bandwidth $\Omega = 2N\Delta\omega$ must be small enough for the instantaneous RF frequency $\dot{\phi}_{RF}(t)$ to be close to the oscillator free-running frequency ω_o.

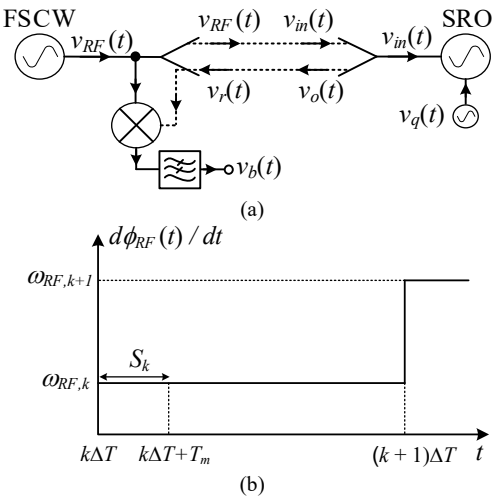

Fig. 1. SRO transponder system. (a) Block diagram. (b). Transmitted frequency-stepped signal.

The SRO, at a distance d from the transmitter, receives the RF input signal: $v_{in}(t) = \alpha(d)v_{RF}(t-\tau) = B\cos\phi_{RF}(t-\tau)$, where $\alpha(d)$ is the attenuation due to the transmission loss, B is the attenuated amplitude, $B = \alpha(d)V_{RF}$, and τ is the time of flight $\tau = d/c$. On the other hand, the oscillation is switched on and off by a low-frequency quench voltage signal that modulates the bias voltage, given by $v_q(t) = V_q\cos(\omega_m t + \phi_m)$, where $\omega_m = 2\pi/T_m$. Note that the oscillation may reach a saturated amplitude before being switched off by $v_q(t)$. In fact, the SRO response will depend on the design and its stability properties, so the modelling of its output voltage $v_o(t)$, addressed in Sub-Section A, is not straightforward. The output voltage $v_o(t)$ is sent to the transmitter, and then mixed (Fig. 1) with $v_{RF}(t)$. The resulting signal is filtered by a low-pass filter to obtain the baseband component:

$$v_b(t) = (v_r(t)v_{RF}(t)) * h(t) \qquad (2)$$

where $v_r(t) = \alpha(d)v_o(t-\tau)$, $h(t)$ is the impulse response of the filter, and $*$ is the convolution operator.

A. Phase response of the standalone SRO

To obtain the SRO model, we will analyse its behaviour when isolated from the transponder system. This analysis will be illustrated through its application to the FET-based oscillator at $\omega_o = 2\pi\cdot 2.76$ GHz shown in Fig. 2. The oscillation is switched on and off with a sinusoidal quench signal $v_q(t)$ introduced in the bias voltage. In each quench cycle $[0, T_m]$, the oscillation is triggered at the time value $t = t_o$ fulfilling $v_q(t_o) = -0.86$ V and switched off when the quench-signal voltage decreases from this value.

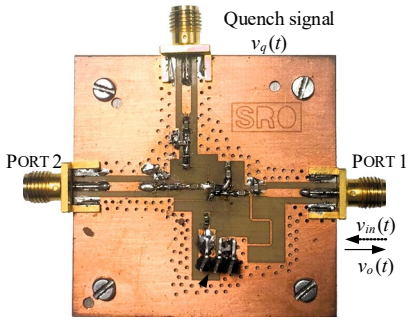

Fig. 2. SRO circuit. The prototype is a FET-based SRO built on Rogers 4003C substrate (ε_r = 3.55 and H = 32 mils). The transistor is an ATF-34143 HEMT. The quench signal $v_q(t)$ is introduced through the gate bias network. Port 1 is used to inject the RF signal $v_{in}(t)$ and extract the output voltage $v_o(t)$. Port 2 is used to monitor the oscillation signal.

In the analysis of the standalone SRO, we will consider the RF input signal $v_{in}(t) = B\cos\phi_{in}(t)$, $\phi_{in}(t) = \omega_{RF}(t-t_o) + \phi_{in,o}$, where B is the input amplitude and $\phi_{in,o}$ is the phase at the start-up time $t = t_o$. The frequencies $\omega_{RF,k} \in [\omega_o - \Omega/2, \omega_o + \Omega/2]$ and ω_o are, in general, much higher that ω_m. Thus, to accurately capture the SRO transient dynamics, we will perform a circuit-level envelope-transient simulation [10], [11] during one quench cycle $[0, T_m]$. As a result, the computational cost is very limited. Note that there is no need to simulate the transponder for the $2N$ frequency steps of time-length ΔT. The simulation is carried out with NH harmonic components, using ω_{RF} as the fundamental frequency. However, due to the oscillator output filtering effects, the SRO output signal can be approached as:

$$v_o(t) \simeq A_o(t)\cos(\omega_{RF}t + \phi_o(t)). \qquad (3)$$

The amplitude term $A_o(t)$ evolves according to the oscillator transient dynamics fulfilling $A_o(t) > 0$ in the oscillation interval $[t_o, t_o + T_s]$. Due to the small-signal input amplitude, it can be assumed to be independent of ω_{RF}. From [12], [13], it can be shown that any constant phase shift in the RF input signal is directly translated to $\phi_o(t)$. Then, the output phase can be expressed as:

$$\phi_o(t) = \phi_{in,o} + \gamma(t, B, \omega_{RF}) \qquad (4)$$

where the function $\gamma(t, B, \omega_{RF})$ models the time-dependence of the phase $\phi_o(t)$ for given values of B and ω_{RF}. The function $\gamma(t, B, \omega_{RF})$ can be extracted through a double sweep in envelope transient. Let $[0, B_{max}]$ be the range of RF input amplitudes considered in the transponder system performance. This range is discretized as $\{B_1, \dots, B_M\}$. For each value B_i, the input RF generator is set to $v_{in}(t) = B_i\cos\omega_{RF}(t-t_o)$ and, since $\phi_{in,o} = 0$, the function $\gamma(t, B, \omega_{RF}) = \phi_o(t)$ is extracted from an envelope simulation during a single quench cycle $[0, T_m]$. The values of $\gamma(t, B, \omega_{RF})$ for any B values in the interval B_1 to B_M can be obtained through linear interpolation. As an example, the functions $\gamma(t, B, \omega_o)$ and $A_o(t)$ resulting from the envelope simulations are shown in Fig. 3. We note the nonlinear time dependence of $\gamma(t, B, \omega_o)$.

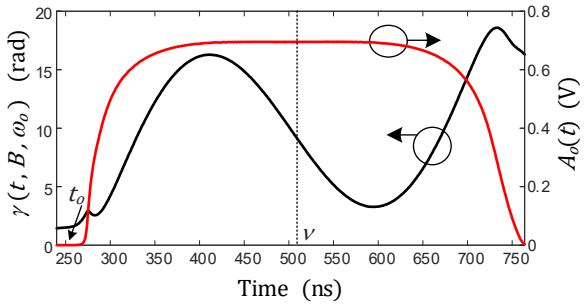

Fig. 3. Simulation of the standalone SRO showing the interval $[t_o, t_o + T_s]$ where $A_o(t) > 0$, with $T_m = 1\,\mu s$ and $\phi_m = \pi$. The resulting functions $\gamma(t, B, \omega_o)$ and $A_o(t)$ for $B = 20\ \mu$V have been represented. The RF input phase at the start-up time $t_o = 253$ ns is $\phi_{in,o} = 0$. The center of the oscillation interval is located at $\nu \equiv t_o + T_s/2 = 507$ ns.

In the SRO transponder, the function $\gamma(t, B, \omega_{RF})$ determines the SRO output phase, which will be combined with that of the transmitter RF source (1) to produce the baseband signal $v_b(t)$. Since $\Omega \ll \omega_o$, we can consider a linear frequency dependence of the function $\gamma(t, B, \omega_{RF})$, which, as shown in the next subsection, will enable the derivation of an analytical expression for $v_b(t)$. Thus, we will express:

$$\gamma(t, B, \omega_{RF}) \simeq \gamma(t, B, \omega_o) + \gamma_\omega(t, B)(\omega_{RF} - \omega_o), \qquad (5)$$

where $\gamma_\omega(t, B) \equiv \partial\gamma(t, B, \omega_o)/\partial\omega$ can be approached by obtaining $\gamma(t, B, \omega_{RF})$ for $\omega_{RF} = \omega_o \pm N\Delta\omega$ and applying finite differences. For the case of Fig. 3, we obtain the $\gamma_\omega(\nu, B) = -510$ ns.

B. SRO transponder system

Next, the behavior of the SRO transponder system will be described in terms of the nonlinear phase function $\gamma(t, B, \omega_{RF})$. According to [1], the time-length ΔT of the stepped-frequency signal in (1) must be significantly longer than the time of flight τ. Here, for simplicity, we will use the relation $\Delta T = 2qT_m$, $q \in Z^+$. Then, the system performance will be analyzed at a set of observation quench cycles $S_k = [k\Delta T, k\Delta T + T_m]$, $k = 0, \dots, 2N$ [Fig. 1(b)]. In each observation cycle S_k, the time variable will be decomposed as $t = k\Delta T + t'$, $t' \in [0, T_m]$. This decomposition allows mapping the SRO response in any observation cycle S_k to the time interval $S_0 = [0, T_m]$. This is derived from the differential equation system fulfilled by the vector of SRO state variables $x(t) = (x_1(t), \dots, x_n(t))$ at each $t \in S_k$. For simplicity of reasoning, we will consider the state-form system $\dot{x}_i(t) = f_i(x(t), t)$, $i = 1, \dots, n$, where $t = k\Delta T + t'$ and $t' \in S_0$. In the following, the notation $x_{i,k}(t') \equiv x_i(k\Delta T + t')$ will be used. These functions fulfil:

$$\frac{dx_{i,k}(t')}{dt'} = \frac{dx_{i,k}(t')}{dt} = f_i(x_k(t'), k\Delta T + t'), \quad (6)$$

where $t' \in S_0$ and $x_k(t') \equiv x(k\Delta T + t')$ and $i = 1, \dots, n$ indicates the particular state variable. Then, the oscillator output voltage in S_k, expressed as $v_{o,k}(t')$, agrees with the signal (3) corresponding to the standalone SRO in $t' \in S_0$ when excited with $v_q(t') = v_{q,k}(t')$ and the RF input signal:

$$v_{in,k}(t') = B\cos(\phi_{RF}(k\Delta T) + \omega_{RF,k}(t' - \tau)). \quad (7)$$

where $\tau < t_o$ has been assumed. Then, from (4) the SRO output phase $\phi_{o,k}(t')$ and amplitude $A_{o,k}(t')$ in S_k are:

$$\phi_{o,k}(t') = \phi_{RF}(k\Delta T) + \omega_{RF,k}(t_o - \tau) + \gamma\big(t', B, \omega_{RF,k}\big), \quad (8)$$

and $A_{o,k}(t') \simeq A_o(t')$ since, as stated in Sub-Section A, the SRO output amplitude is independent of $\omega_{RF,k}$. Using (3) and (8), the baseband signal (2) in $t' \in [t_o + \tau, t_o + T_s + \tau]$ can be approached as:

$$v_{b,k}(t') \simeq V_b(t' - \tau)\cos\Big(\omega_{RF,k}(2\tau - t_o) - \gamma\big(t' - \tau, B, \omega_{RF,k}\big)\Big) \quad (9)$$

where $V_b(t') \equiv BA_o(t')/2$. Note that it has been assumed that the low-pass filter removes the high-order frequency components of the mixer output. Next, in each S_k the signal $v_{b,k}(t')$ is sampled at $t' = t_s$ lying in the center of the received symbol. Thus, the sampling time can be expressed as $t_s = \nu + \tau$, where $\nu \equiv t_o + T_s/2$. Considering this sampling time in (9):

$$\tilde{v}_{b,k} \equiv v_{b,k}(t_s) = V_b(\nu)\cos\big(\omega_b(\tau)k\Delta T + \phi_b(\tau)\big), \quad (10)$$

where the approximation (5) has been considered, and:

$$\omega_b(\tau) \equiv \mu\big(2\tau - t_o - \gamma_\omega(\nu, B)\big). \quad (11)$$

The phase $\phi_b(\tau)$ in (10) takes the same value for all the samples, given by:

$$\phi_b(\tau) \equiv \omega_b(\tau)\left(\frac{\omega_o}{\mu} - N\Delta T\right) - \gamma_o(\nu, B) + \gamma_\omega(\nu, B)\omega_o, \quad (12)$$

where $\gamma_o(\nu, B) \equiv \gamma(\nu, B, \omega_o)$. Thus, the set of samples $\tilde{v}_{b,k}$ at $k\Delta T$, where $k = 0, \dots, 2N$ conform a periodic sinusoidal signal with frequency $\omega_b(\tau)$. Therefore, the sampled waveform (10) provides the baseband frequency ω_b resulting for each distance $d = c\tau$. In the measurement, this frequency is simply obtained by applying the FFT operation to the set of samples. Then, the distance $d = c\tau$ is derived from (11) using the values t_o, ν and $\gamma_\omega(\nu, B)$. These values are independent of the time-of-flight τ, so they can be calculated from the analysis or measurements of the standalone SRO during a single quench cycle (see Fig. 3). Note that expressions (11) and (12) particularize to the ones in [1] when considering the linear approach $\gamma(t, \omega_{RF}) = (\omega_o - \omega_{RF})t - \omega_o t_o$. This serves as a comparison between the two models. Note that the influence of the nonlinearity in $\gamma(t, B, \omega_{RF})$ will be larger for a shorter oscillation interval, since the SRO instantaneous frequency will be less stabilized.

To validate the model, we have used a stepped frequency modulated signal with $N = 40$ steps of size $\Delta\omega = 200$ kHz, time between steps $\Delta T = 1\mu s$, and amplitude $B = 20\ \mu V$. The time delay is $\tau = 40$ ns, corresponding to $d = 12$ m, and the frequency of the sinusoidal quench signal is $f_m = 1$ MHz. With these data, the SRO transponder has been simulated with envelope transient considering $NH = 7$ harmonic terms. Fig. 4 shows the first 16 samples, $\tilde{v}_{b,k}$, of the resulting baseband signal $v_b(t)$. The samples conform a periodic signal at the frequency $\omega_b(\tau) = 2\pi \cdot 67$ kHz. Introducing this frequency in (11) (with $\gamma_\omega(\nu, B)$ calculated in the standalone SRO) we obtain the prefixed value $\tau = 40$ ns, which validates the model.

Next, the SRO transponder has been measured for $d = 12$ m using the test bench in Fig. 5. The RF signal is generated with a VSG60A Generator. The quench signal is generated with the Agilent 8118B Arbitrary Waveform Generator. In the transmitter, a sample of the RF signal is mixed with the received signal using a ZEM-4300+ mixer. At the mixer output, the high-frequency components are filtered with a SLP-10.7+ Low Pass Filter and the baseband signal is recovered with an Agilent DSO90804A Oscilloscope. The first 16 samples of the sampled baseband signal are superimposed in Fig. 4. They agree with the ones obtained in simulation. Then, using $\gamma_\omega(\nu, B)$ of the standalone SRO we obtain again the prefixed value $d = 12$ m.

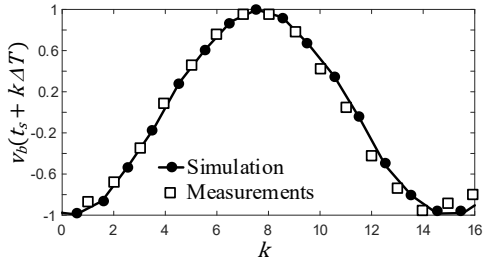

Fig. 4. Normalized sampled baseband signal for $d = 12$ m. Comparison of the simulated and measured samples $\tilde{v}_{b,k} \equiv v_b(t_s + k\Delta T)$. The value $d = 12$ m extracted from this sampled signal using (11) (with $\gamma_\omega(\nu, B)$ calculated in the standalone SRO) agrees with the distance used in the simulation and in the measurement.

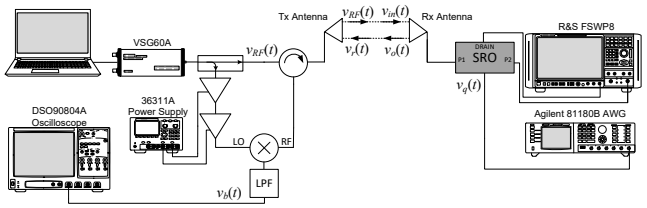

Fig. 5. Schematic of the test-bench. Measurements superimposed in Fig. 4.

III. Conclusions

A realistic modeling method for active transponders based on super regenerative oscillators has been presented. It is based on the extraction of a phase function from an envelope-transient simulation of the oscillator circuit during a single quench cycle. After mixing and filtering, the analysis provides an accurate relationship between the frequency of the sampled baseband signal and the distance to the target. The predictions have been successfully validated with envelope-transient simulation of the complete transponder operation and experimental measurements.

Acknowledgment

This work was supported by the Spanish Ministry for Science and Innovation under the research project PID2020-116569RB-C31.

References

[1] M. Vossiek and P. Gulden, "The Switched Injection-Locked Oscillator: A Novel Versatile Concept for Wireless Transponder and Localization Systems," *IEEE Trans. Microw. Theory Tech.*, vol. 56, no. 4, pp. 859–866, 2008, doi: 10.1109/TMTT.2008.918158.

[2] M. V Thayyil, S. Li, N. Joram, and F. Ellinger, "A K -Band SiGe Superregenerative Amplifier for FMCW Radar Active Reflector Applications," *IEEE Microw. Wireless Compon. Lett.*, vol. 28, no. 7, pp. 603–605, 2018, doi: 10.1109/LMWC.2018.2839063.

[3] P. Palà-Schönwälder, J. Bonet-Dalmau, F. X. Moncunill-Geniz, F. del Águila-López, and R. Giralt-Mas, "A Superregenerative QPSK Receiver," *IEEE Trans. Circuits Syst. I, Reg. Papers*, vol. 61, no. 1, pp. 258–265, 2014, doi: 10.1109/TCSI.2013.2268313.

[4] F. X. Moncunill-Geniz, J. Bonet-Dalmau, F. Del Águila-Lopez, I. Demirkol, and P. Palà-Schönwälder, "Super-Regenerative Receiver for OFDM Communication," in *IEEE Int. Symp. Circuits Syst. (ISCAS)*, 2022, pp. 1843–1847. doi: 10.1109/ISCAS48785.2022.9937447.

[5] L. Hahn, M. Vossiek, and C. Carlowitz, "A Low-Power, Subharmonic Super-Regenerative Receiver toward a Massive Multichannel FMCW Radar Close to Cut-Off Frequency," in *IEEE MTT-S Int. Microw. Symp. Dig.*, 2023, pp. 513–516. doi: 10.1109/IMS37964.2023.10188187.

[6] M. Schtz, Y. Dobrev, C. Carlowitz, and M. Vossiek, "Wireless Local Positioning with SILO-Based Backscatter Transponders for Autonomous Robot Navigation," in *IEEE MTT-S Int. Conf. Microw. Intell. Mobil. (ICMIM)*, 2018, pp. 1–4. doi: 10.1109/ICMIM.2018.8443524.

[7] L. Hahn, M. Vossiek, and C. Carlowitz, "A Subharmonic Super-Regenerative FMCW Radar With Improved Intermodulation Efficiency for Applications Beyond Cut-Off Frequency," *IEEE Trans. Microw. Theory Tech.*, pp. 1–15, 2023, doi: 10.1109/TMTT.2023.3316305.

[8] M. Schütz, Y. Dobrev, T. Pavlenko, and M. Vossiek, "A Secondary Surveillance Radar with Miniaturized Transponders for Localization of Small-Sized UAVs in Controlled Air Space," in *5th IEEE Int. Workshop on Metrology for AeroSpace (MetroAeroSpace)*, 2018, pp. 107–111. doi: 10.1109/MetroAeroSpace.2018.8453580.

[9] H. Ghaleb, N. Joram, and F. Ellinger, "A 60-GHz Super-Regenerative Oscillator with 80 dB Gain in SiGe BiCMOS for FMCW Radar Active Reflectors," in *IEEE 22nd Topical Meeting on Silicon Monolithic Integrated Circuits in RF Systems (SiRF)*, 2022, pp. 31–34. doi: 10.1109/SiRF53094.2022.9720047.

[10] E. Ngoya and R. Larcheveque, "Envelope transient analysis: A new method for the transient and steady-state analysis of microwave communication circuits and systems," *IEEE MTT-S Int. Microw. Symp. Dig.*, 1996.

[11] N. B. Carvalho, J. C. Pedro, W. Jang, and M. B. Steer, "Simulation of nonlinear RF circuits driven by multi-carrier modulated signals," in *IEEE MTT-S Int. Microw. Symp. Dig.*, Long Beach, CA, United States, Jun. 2005, pp. 801–804. doi: 10.1109/MWSYM.2005.1516736.

[12] S. Hernández and A. Suárez, "Analysis of Superregenerative Oscillators in Nonlinear Mode," *IEEE Trans. Microw. Theory Tech.*, vol. 67, no. 6, pp. 2247–2258, 2019, doi: 10.1109/TMTT.2019.2910014.

[13] S. Hernández and A. Suarez, "Envelope-domain analysis and modeling of super-regenerative oscillators," *IEEE Trans. Microw. Theory Tech*, vol. 66, no. 8, pp. 3877–3893, Aug. 2018, doi: 10.1109/TMTT.2018.2836397.